

## Chapter 6

# Multi-component Data Equalization

In this chapter I attempt to correct the previously-discussed data set that showed extreme energy variations (Chapter 2) and largely non-reciprocal behavior (Chapter 4) so that the data become more reciprocal. In Chapter 3 I defined the problem theoretically and gave a numerical analysis of the solution structure by treating it as a generalized inverse problem. In this chapter I apply it to a small synthetic transverse isotropic (TI) data set that is based on the Marmousi structural model and show that the equalization gives results as theory would predict. When I apply it to the nine-component data, the equalization improves data symmetry for strong coherent events.

### 6.1 The optimization problem

In chapter 3 I described the solution structure to the problem of finding the symmetric data in an optimal way. In this chapter I set up a least-squares optimization problem in which I minimize the difference between data and its reciprocal counterpart. Analysis of the solution structure of the problem shows that none of the eigenvectors has a pure spatial DC component. Thus, the absolute radiation pattern at source and receiver locations cannot be determined. However, relative changes should be resolved within a cable length. This relativity requires one to specify a reference with respect to which the prediction error or matching filters are computed. In the optimization I equalize to the average of the reciprocal trace pairs. Thus, source and receiver behavior influence the estimation

in equal proportions. My initial guess to the solution is a single spike at the zero-lag filter location, while in the subsequent minimization process the filter coefficients are not constrained at all.

I find the global minimum of the squared difference for the filtered trace pairs, allowing for  $E$  to represent the total misfit of filtered data samples:

$$E = \sum_{i,j,k,l} \{d_{ji}^{lk} * s_j^{lk} - d_{ij}^{kl} * s_i^{kl}\}^2. \quad (6.1)$$

The indices  $i$  and  $j$  range over all the different source and reciprocal source locations and the indices  $l$  and  $k$  (source and reciprocal source components) both remain within the range 1 to 3. The values of  $i$  and  $j$  can describe source location in 2-D or 3-D. Convolution is denoted by  $*$ . For each source location, the general shape of  $s^{kl}$  in  $E$  is

$$\begin{pmatrix} s_{11}(t) & s_{12}(t) & s_{13}(t) \\ s_{21}(t) & s_{22}(t) & s_{23}(t) \\ s_{31}(t) & s_{32}(t) & s_{33}(t) \end{pmatrix}.$$

A filter pair,  $s_i^{kl}$  and  $s_j^{lk}$ , applies to a trace pair ensemble. In equation (6.1),  $s$  is estimated as a short function in time for each source component pair. The choice of this form of parameterization allows one to characterize differences in source and receiver behavior as wavelet changes depending on the direction of force applied to the free surface, and not merely as simple impedance amplitude scaling.

## 6.2 Synthetic equalization examples

### 6.2.1 Two noisy spikes

To illustrate the optimization procedure, I generated two presumably reciprocal seismic traces, as shown in the left part of Figure 6.1. Each of traces consists of an isolated band-limited event with about 20% random noise added. One event is a Ricker wavelet with a bandwidth of 5-30 Hz; the other is time shifted by about five samples and has a bandwidth of 10-50 Hz. Assuming that the reciprocal trace pair is generated by two different experiments, I design one-dimensional filters to remove their differences. Note that the effective bandwidth overlap is 10-20 Hz only. The equalization filters are each a total of 40 points long and are initialized with a single spike at zero lag time. The right-hand plot in Figure 6.1 shows the equalized traces after about 40 iterations; the

filters themselves are shown in Figure 6.2. The first filter is constrained to have a peak maximum of unit amplitude at zero lag. Thus the first trace is favored to be close to the true trace. The main event after equalization matches well. The filter for the reciprocal trace incorporates correctly a shift of the original event and also a modification of the signals spectrum to match the first trace. The additive noise in the second trace is not completely random anymore, but shows some frequency characteristic since it was filtered with the equalization filter.

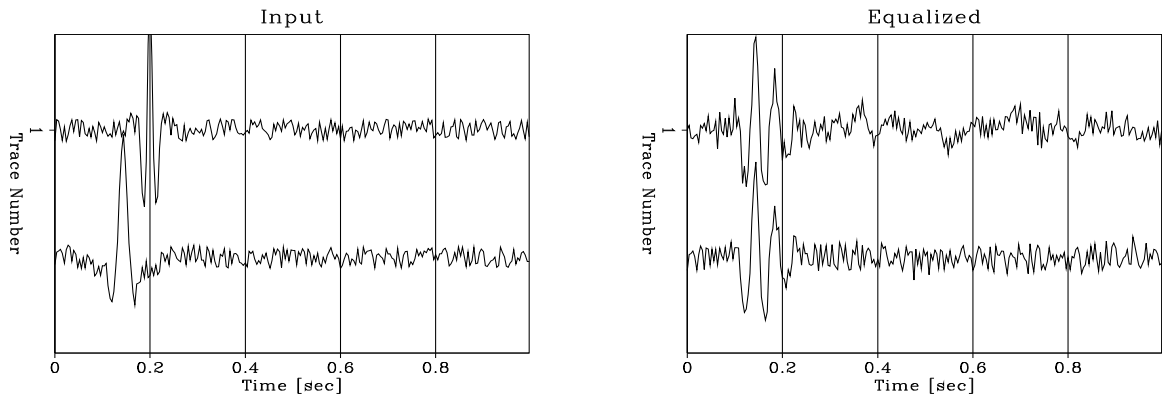


FIG. 6.1. Two traces with different events are generated and constitute a reciprocal trace pair. The random noise level is 20 % of the peak signal. The left plot shows the traces that are equalized with the use of the filters shown in Figure 6.2. `srceq-wavelet2N` [R]

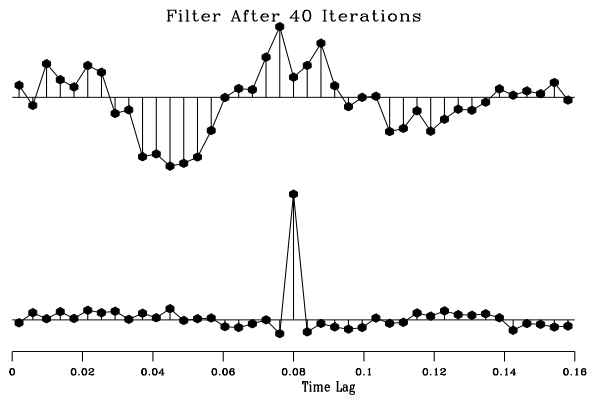


FIG. 6.2. Filter after 40 iterations. The reciprocal trace pair in Figure 6.1 is equalized, so that only 7% residual mismatch energy is left after 40 iterations using this filter pair.

`srceq-filt2N` [R]

### 6.2.2 Transverse Isotropic Marmousi

To test the equalization procedure on a more realistically-modeled dataset, I use ten four-component shot gathers that are forward modeled in 2-D, with the finite-difference method described in Chapter 5. I restrict myself to ten shot gathers, since I analyzed the solution behavior of this particular case in Chapter 3. The Marmousi subsurface velocity model serves as structural background model. I augment the original acoustic specification by creating a fully transverse isotropic medium of such a nature that its properties vary consistently with the interfaces in the originally prescribed structure. The velocity anisotropy along the vertical and horizontal direction varies randomly up to 10% between different lithological units. Additionally, I replace the original constant water velocity layer by a heterogeneous near surface layer with a random spatial variability. Figure 6.3 shows a typically generated wavefield; most noticeable are the strongly diffracting low-velocity surface waves caused by the extremely complex near surface.

All ten shot gathers were generated with different source behavior. The first shot is carried out with a source of a fundamental frequency of 15 Hz, rolling off in the high frequency band. Various other shots have their frequency range limited to 10-25 Hz, 20-50 Hz, or 2-15 Hz. Two of them have also static time shifts of 30 msec and 60 msec applied. Three shots are limited in source strength to 10%, 70%, and 200%. Finally, the last shot has uniform random noise superimposed on all gathers.

Figure 6.5 shows a spectral characterization of the various source differences in the frequency range up to 60 Hz. The first shot is the reference/average shot and shows a zero deviation. The second one has most of its differences in the band between 5 Hz and 30 Hz. The third, fifth, and seventh shot show differences along the entire frequency band; their deviation from the reference are caused by combinations of mere amplitude scaling and static shifting. The fourth and sixth shot differences are relatively low-frequency band-limited, while shots eight and nine are high-frequency band-limited. The tenth shot shows random variations over the entire frequency band. An important point is that the frequency content of those differences overlaps with frequency content of the reference shot. If they share approximately the same spectral band, then an estimation can proceed successfully. But if there is only minimal overlap the optimization concentrates on equalizing that particular coincident frequency band, while leaving the remaining spectral parts unequalized. If the spectra do not overlap at all, then the equalization is ill-conditioned and not practical to carry out. In Figure 6.6 the collection of four-component reciprocal

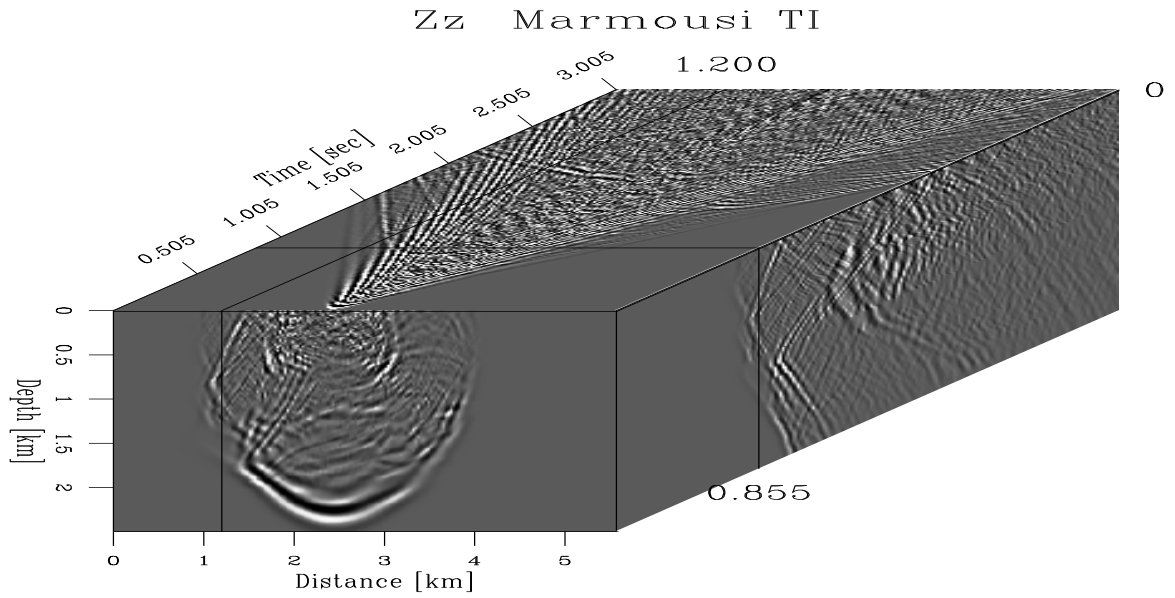


FIG. 6.3. Ten shot are modeled in a Marmousi model that has been extended to a transverse isotropy. The  $Zz$  component of the recording is shown in this picture. `srceq-zsnap.demo` [CR]

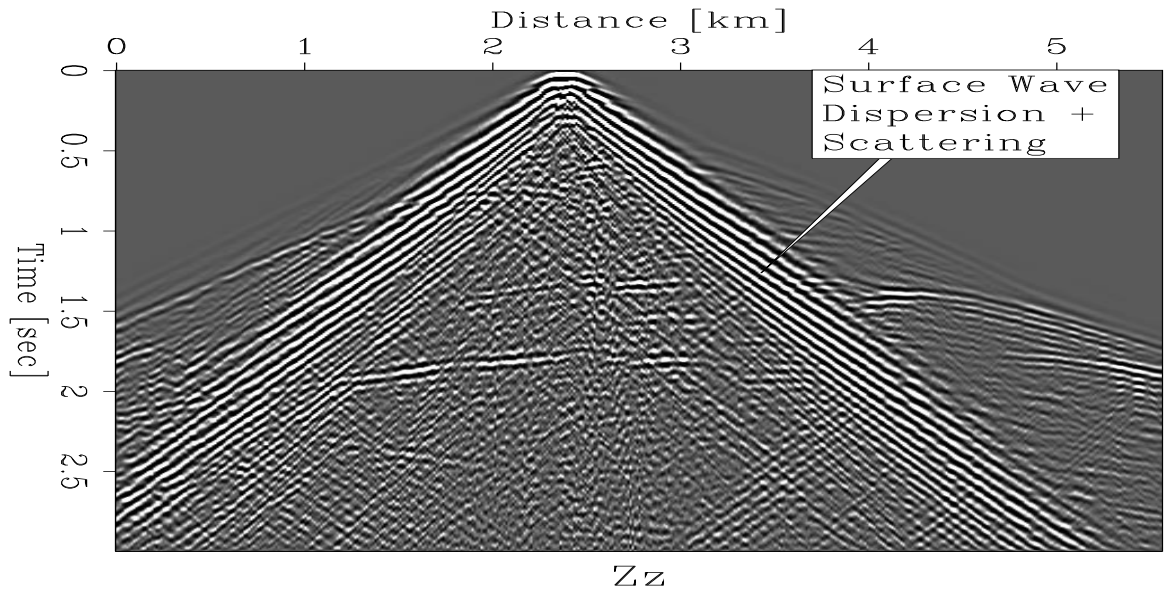
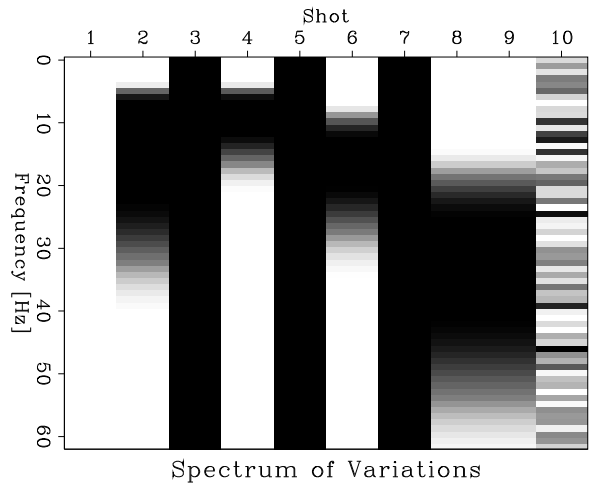


FIG. 6.4. The  $Zz$  component of a seismogram is modeled through a transverse isotropic Marmousi subsurface structure. The usual water layer is replaced in this model with an extremely variable near surface layer. Thus it generates strong surfaces waves that themselves show scattering effects off near-surface heterogeneities. This pattern is superimposed onto the subsurface reflections that one is normally used to seeing on conventional acoustic Marmousi shot gathers. `srceq-seismo` [CR]

traces are displayed for the entire experiment. Each reciprocal trace carries information about its source behavior and about the reflectivity characteristic within the medium itself. Therefore there is no direct correspondence to the different source behavior, as shown in 6.5, but rather the general influence on the collection of reciprocal traces within a shot is noticeable. Figure 6.7 shows the reciprocal trace gathers generated with identical sources. This is what the optimization algorithm ideally should achieve.

FIG. 6.5. Ten synthetic shots have variations from an average shot. The differences have various spectral bandwidth and amplitude. Some of the variations hardly overlap, while others show an effect over a large frequency band. `srceq-diffspec` [CR]



In Figures 6.8 reciprocal trace pairs are equalized with a limit of 5 iterations during optimization. The filters are obtained after a limit of five iterations and the resulting traces match the reciprocal traces quite well for all four components. This procedure has some difficulty balancing traces that belong to shot eight and nine since the spectral overlap with the average is very small. The whole data set is still not quite equalized, but individual trace pairs are. At the same time as individual differences are evened out, general energy levels are simultaneously equalized. The data in Figure 6.8, after equalization to an average energy level, appear as if they had been uniformly generated, but they still differ from the data with no source variations applied, as shown in Figure 6.7.

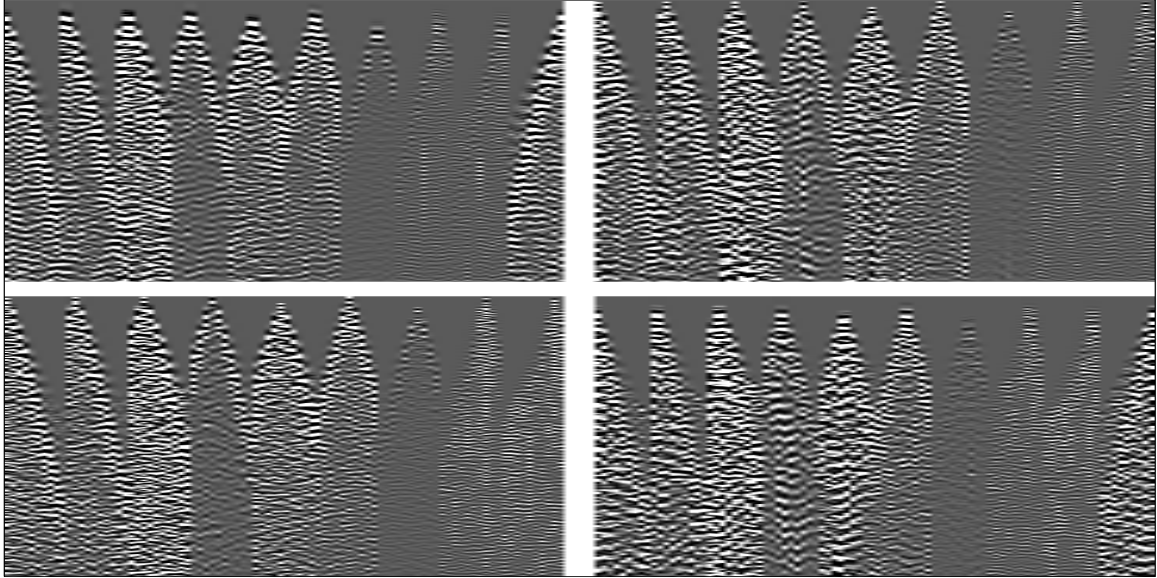


FIG. 6.6. Reciprocal traces were extracted from the ten four-component shots. Variations in the traces due to spatial variations in source behavior are visible on all components.

`srceq-before` [CR]

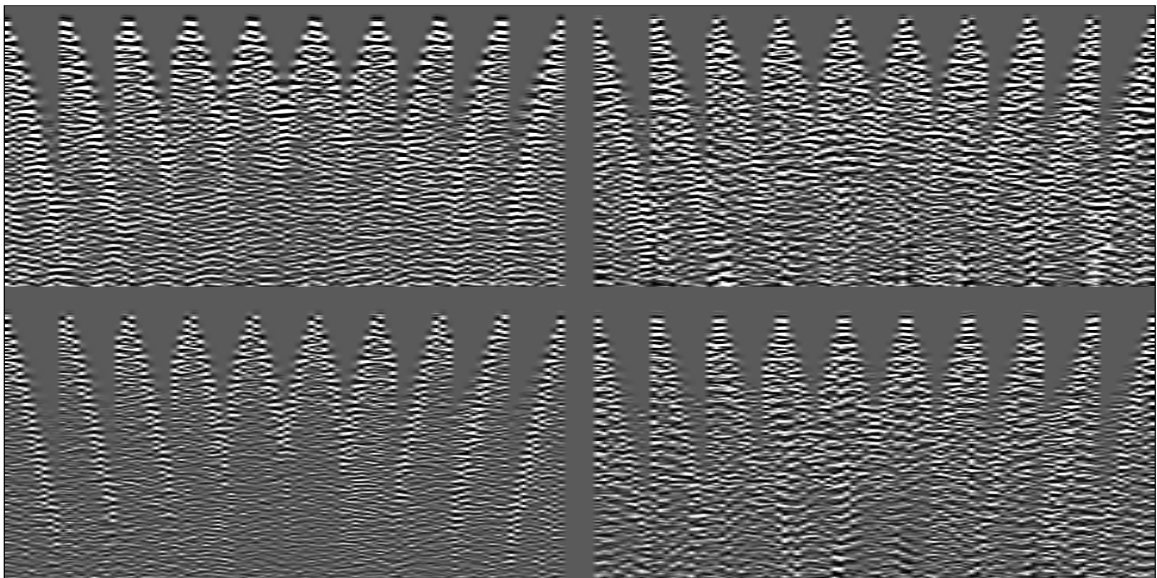


FIG. 6.7. Reciprocal traces were extracted from the ten four-component shots that were generated with identical sources. This is the aim of data equalization.

`srceq-novar` [CR]

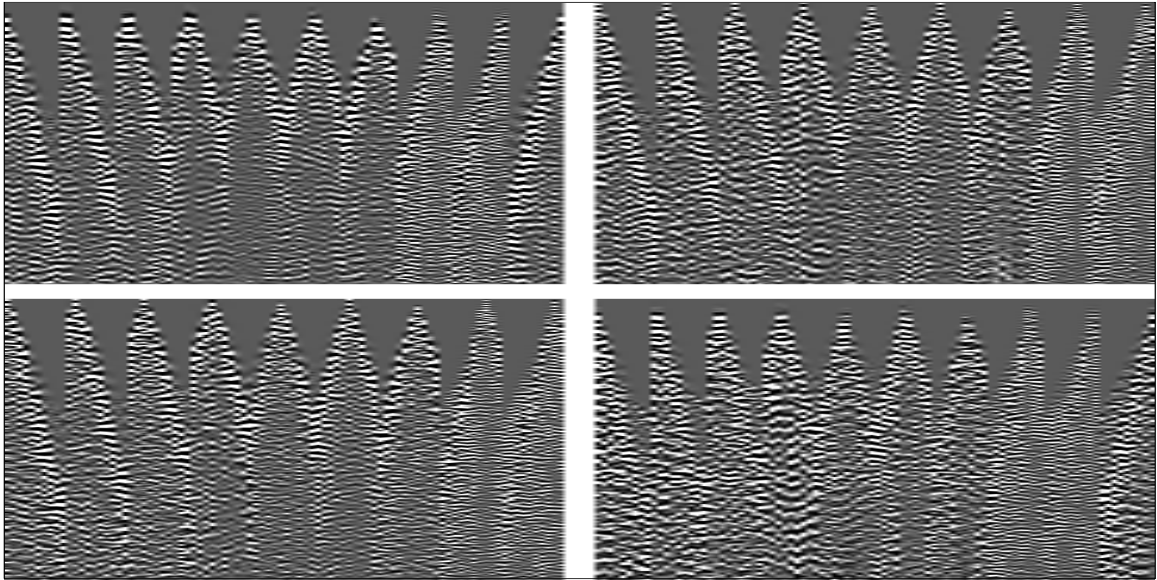


FIG. 6.8. Reciprocal traces were extracted from the ten four-component shots and equalized using matching filter designed for each individual trace pair after the energy level in the trace was optimally matched with a limit of five iterations. `srceq-xquizsyntB` [CR]

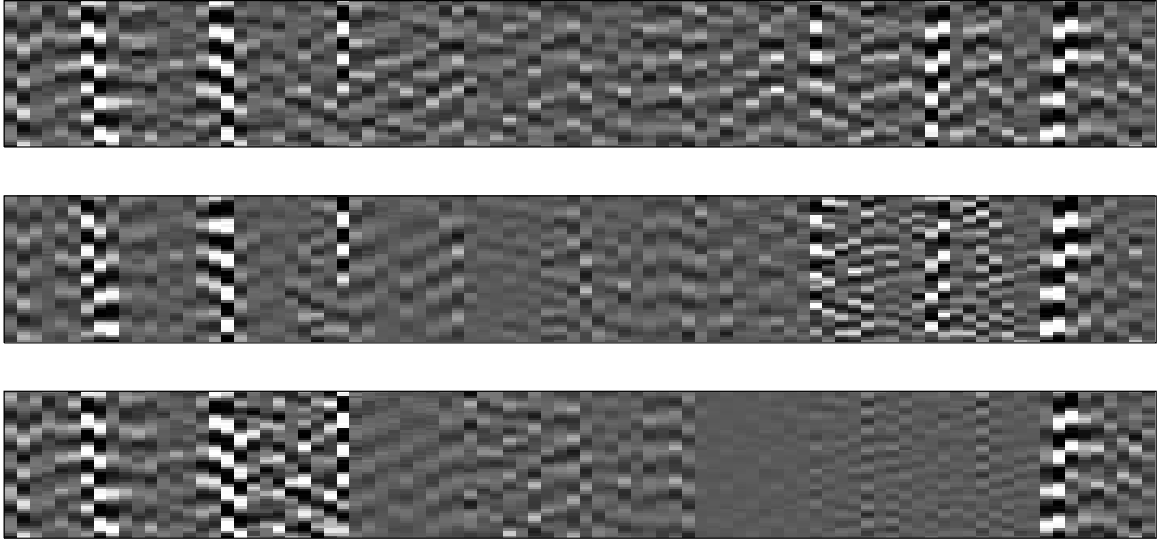
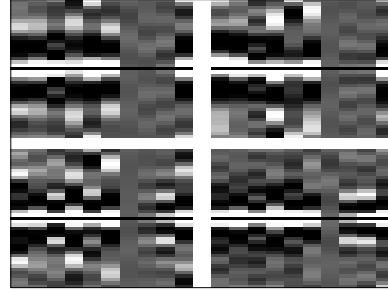


FIG. 6.9. Reciprocal traces were extracted from the ten four-component shots and equalized using matching filter designed for each individual trace pair after the energy level in the trace was optimally matched with a limit of five iteration. The top plot shows the data obtained with no source variations; the middle plot shows the data resulting from reciprocal equalization and the bottom plot shows the data with source variations. The equalization finds approximately the right amplitude level, but deviates still a small amount in the frequency character of some events; however it is an improvement compared to the unequalized data. `srceq-windowxx` [CR]

FIG. 6.10. Four-component equalization filters for individual sources. `sreceq-filtras` [CR]



The optimization is able to find a reasonable equalization of the numerically simulated prestack data in a limited number of iterations. I chose a realistic synthetic model that includes anisotropy and near-surface variations. The reciprocal trace pair optimization produces a result consistent with the data without source variations.

### 6.3 Equalizing a nine-component land data set

The data set I used in Chapter 2 and 4 shows strong spatial variations in signal energy and to a large degree lack of reciprocity. In order to counterbalance such signal behavior, I apply the equalization technique that I tested in the previous section on the numerically simulated TI Marmousi test data.

I used 20-point long 1-D filters to equalize a 3-4 second time window of the entire prestack data set. The equalization technique uses a conjugate gradient optimization technique to find the best matching filter for each trace pair in the data cube and levels the amplitude to an average energy level. Figure 6.11 shows a comparison of the  $Yy$  component before and after equalization. The top sub-plot displays the NMO-corrected prestack data set before equalization. The sub-plot consists of three individual panels that are obtained by cutting the data cube along fixed planes. The top panel shows a slice of constant time at 3.12 seconds. One can see symmetry along the vertical axis (midpoint axis) mostly for the curved main event and, to a lesser degree, for linear events visible in the lower midpoint region. For the higher midpoint region the signal amplitude level drops off rapidly and only faint features are visible. The panel below the time slice is a cut through the data set at a fixed midpoint location; the side panel is a constant offset section.

The top figure contrasts with the bottom figure, where the optimum-matched filter

equalization has been applied. The prestack data cubes are displayed at identical times and locations. The main difference in the bottom plot is the equalization to an overall amplitude level that has less spatial variation than the top plot. The curved event in the middle of the time slice, which already was quite symmetric, is improved in that the amplitudes are more spatially coherent from zero up to maximum offset. The largest effect, however, is visible in the region for higher midpoint numbers in the upper part of the plots. After equalization, the signal level is coherently and symmetrically increased over a broad region. The X-shaped patterns faintly visible in the unequalized time slice are now symmetrically equalized to the general signal level.

The comparisons of the midpoint gathers show a uniform signal strength and character. The 1-D filter was able to suppress some of the large-amplitude high-frequency traces, while at the same time increase the signal level in regions of unequal lower amplitude. The symmetry with respect to the midpoint axis is increased. One observes the same behavior in the constant offset gathers. The signal along the midpoint axis appears more balanced with a uniform signal character.

The following Figures 6.12 and 6.11 adhere to the same display method for reciprocal traces, as shown in Figure 4.8, with the midpoint axis extending vertically downwards in the middle of the sub-plots and with an expected symmetry with respect to the midpoint axis. Figure 6.12 displays for all nine components an unbalanced time slice at a time coincident with the  $Yy$  component in Figure 6.11 and findings for the  $Yy$  component agree generally with the  $Xx$  component. The horizontal cross-components  $Xz$  and  $Zx$  show a balanced level of amplitude distribution in regions where there was low signal energy. However, coherent energy is mostly in the curved event in the middle of the plot.

Particularly in the lower part, the  $Zz$  component exhibits signal energy that is largely coherent over long offset ranges within a few midpoints. The equalization finds that behavior to be reciprocally consistent and enhances and balances those patterns over the entire  $Zz$  dataset. On the remaining cross components  $Xz$ ,  $Yz$ ,  $Zxy$  and  $Zy$  hardly any coherent event can be found. The equalization does its best to increase symmetry, but an increase in coherency is absent.

The results of data equalization using the reciprocity criterion show that symmetry in the prestack data is increased where coherent reflection events are present. Where they are not, the equalization does its best to symmetrize the data, thereby effectively equalizing the energy level. Pure source and pure receiver consistent effects are evened out in this

process in such a way that they are suppressed or reappear in a symmetric manner. The equalization did not reveal any hidden coherent events. The source and receiver property variability in this data set is very strong and I concluded that no attention had been paid to performing a true reciprocal experiment. Moreover, the source behavior for the free-surface impact source is not characterizable with only a single scalar number, as it would be with a simple impedance mismatch. Rather it is different for all nine components and, considering the low data quality, I restricted myself to characterizing non-reciprocal variations with simple 1-D filters in time for each of the components.

## **6.4 Summary**

Equalization of numerically simulated data, based on a transverse isotropic Marmousi model with a variable near-surface, shows results as the analytical solution analysis would predict. No subsurface information such as velocity, density, or stiffness is necessary for performing the prestack equalization with 1-D filters in time. I applied the same technique to a nine-component land data set and found that the algorithm equalizes coherent events and in general evens out the energy level in the prestack data. The variability in the original data is great and equalization does not reveal hidden events that are traceable; for this same reason, a conclusion about the typical source and receiver behavior is not possible.

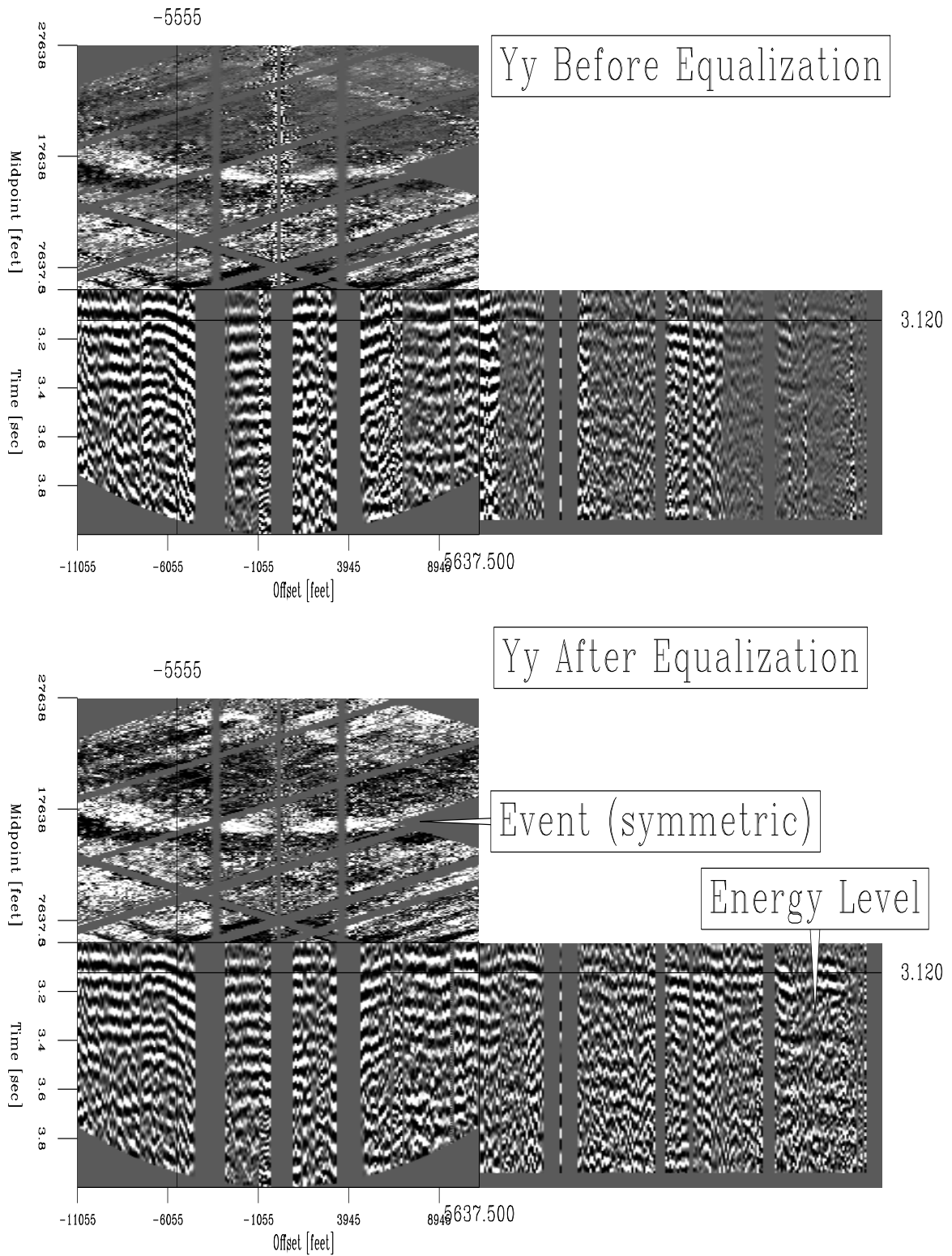


FIG. 6.11. The  $Yy$  component is displayed before and after equalization in a time window from 3-4 seconds. The data equalization has increased the symmetry along the strong event in the middle of the time slice and, for higher midpoints the general level of reflections are more symmetrically increased. Equalization is also visible along the side panel in the constant offset section and in the front panel, that is the midpoint gather.

srceq-eqyycube [R]

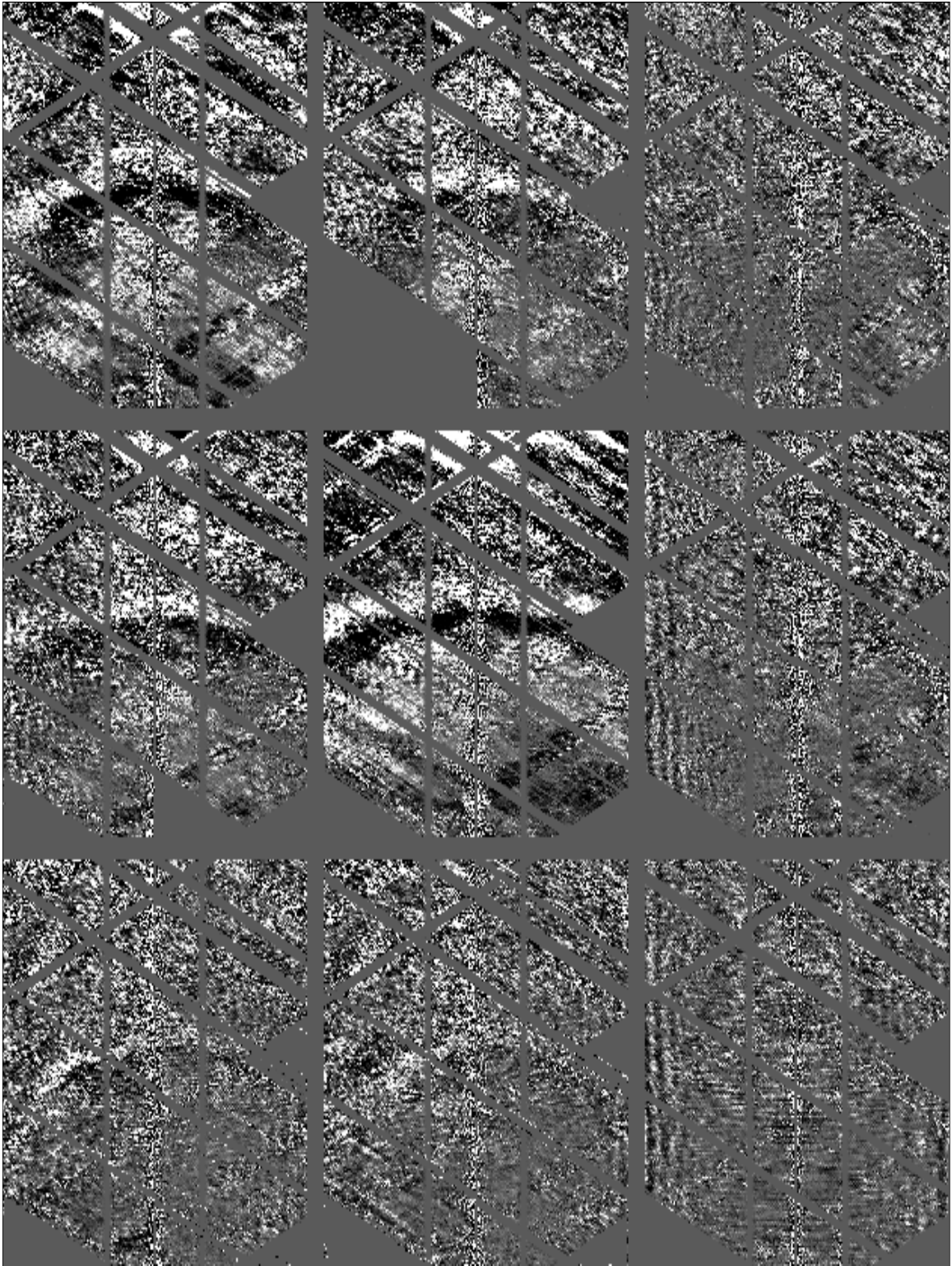


FIG. 6.12. A time slice at 3.12 seconds after NMO is applied. `srceq-recinmo` [R]

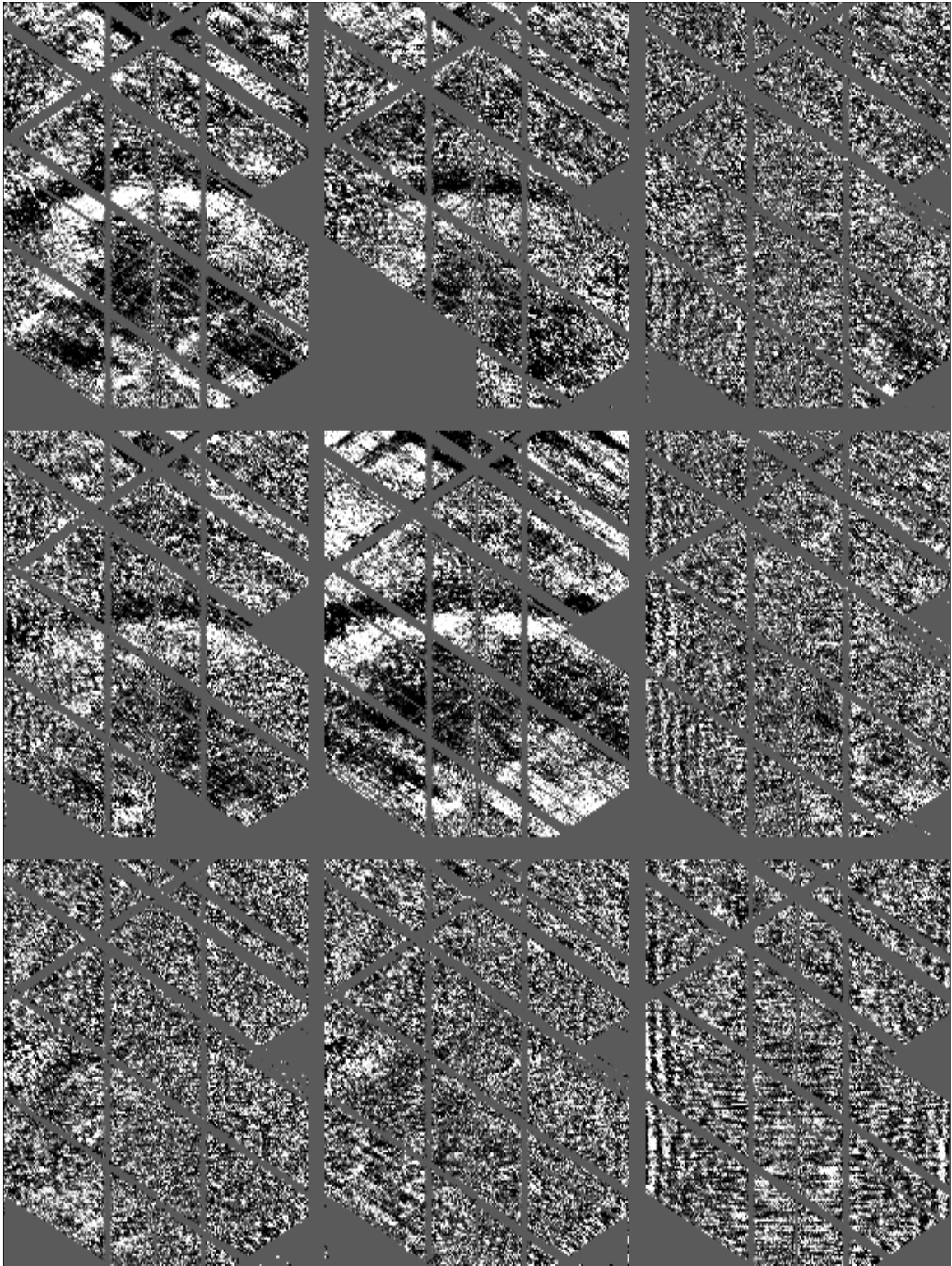


FIG. 6.13. A time slice is equalized on individual trace pairs for a time window between 3 and 4 seconds with NMO applied to the resulting data. srceq-xquizNMOBAVr [R]